Inorganic Chemistry

Article

pubs.acs.org/IC

$Gd_4Ge_{3-x}Pn_x$ (Pn = P, Sb, Bi, x = 0.5−3): Stabilizing the Nonexisting Gd_4Ge_3 Binary through Valence Electron Concentration. Electronic and Magnetic Properties of $Gd_4Ge_{3-x}Pn_x$

Yan Yin Janice Cheung,[†] Volodymyr Svitlyk,[‡] and Yurij Mozharivskyj*[,†]

[†]Department of Chemistry and Chemical Biology, McMaster University, Hamilton, Ontario, L8S 4M1, Canada

[‡]Institut für Anorganische und Analytische Chemie, Universität Münster, Corrensstrasse 30, D-48149 Münster, Germany

Supporting Information

ABSTRACT: $Gd_4Ge_{3-x}Pn_x$ (Pn = P, Sb, Bi; x = 0.5−3) phases have been prepared and characterized using X-ray diffraction, wavelength-dispersive spectroscopy, and magnetization measurements. All $Gd_4Ge_{3-x}Pn_x$ phases adopt a cubic anti-Th_3P_4 structure, and no deficiency on the Gd or p-element site could be detected. Only one P-containing phase with the $Gd_4Ge_{2.51(5)}P_{0.49(5)}$ composition could be obtained, as larger substitution levels did not yield the phase. Existence of $Gd_4Ge_{2.51(5)}P_{0.49(5)}$ and $Gd_4Ge_{2.49(3)}Bi_{0.51(3)}$ suggests that the hypothetical Gd_4Ge_3 binary can be easily stabilized by a small increase in the valence electron count and that the size of the p element is not a key factor. Electronic structure calculations reveal that large substitution levels with more electron-rich Sb and Bi are possible for charge-balanced $(Gd^{3+})_4(Ge^{4-})_3$ as extra electrons occupy the bonding Gd−Gd and Gd−Ge states. This analysis also supports the stability of Gd_4Sb_3 and Gd_4Bi_3. All $Gd_4Ge_{3-x}Pn_x$ phases order ferromagnetically with relatively high Curie temperatures of 234−356 K. The variation in the Curie temperatures of the $Gd_4Ge_{3-x}Sb_x$ and $Gd_4Ge_{3-x}Bi_x$ series can be explained through the changes in the numbers of conduction electrons associated with Ge/Sb(Bi) substitution.

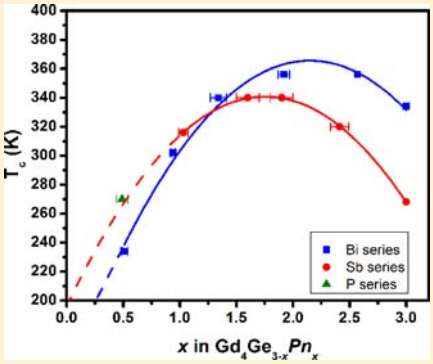

INTRODUCTION

The rare-earth binary and pseudobinary phases of group 14 and 15 elements, as well as their derivatives, have gained a lot of attention[1−6] since the discovery of the giant magnetocaloric effect (GMCE) in pseudobinary $Gd_5Si_{4-x}Ge_x$ phases.[7−10] One of the important outcomes of such research is the possibility of tuning the structural and magnetic properties of the RE_5X_4 phases (RE is a rare earth and X a p element) through valence electron concentration.[4,11−15] For example, a decrease in the valence electron count in Gd_5Ge_4 through Ga substitution leads to formation of the interslab dimers and temperature-induced structural transitions concomitant with a giant magnetocaloric effect in $Gd_5Ge_{4-x}Ga_x$.[11,15] For the most part, research in this area appears to focus primarily on the RE_5X_4 phases with little attention given to other binary phases or their derivatives. While such preoccupation with one type of material is fully understood, the rare-earth and group 14 and 15 elements offer a variety of other binary phases with different magnetic properties.[16] However, the structure and properties of such phases appear to be less systematically studied, and in general, the factors governing their stability are not as well understood.

If we were to limit our attention to the rare-earth-rich side of the binary diagrams, we could see an interesting trend regarding the existence of RE_5X_3 (Mn_5Si_3 structure), RE_4X_3 (anti-Th_3P_4 structure), and RE_5X_4 (Sm_5Ge_4, Gd_5Si_4, or Zr_5Si_4 structures) phases (RE is a rare earth element, X is Si, Ge, Sn, Sb, Bi). With the exception of Ce_3Si_2, $(La/Ce/Pr)_4Ge_3$, La_3Sb_2, and few other binaries, the general trend is that RE_5X_3 and RE_5X_4 phases exist for tetralides and RE_5X_3 and RE_4X_3 ones for pnictides. Thus, while the RE_5X_3 phases are stable both for tetralides and for pnictides, the RE_5X_4 and RE_4X_3 ones exist with either tetralides or pnictides, respectively. The size factor does not appear to play a role, as exchanging Sb for size-similar Sn yields RE_4Sb_3 instead of RE_5Sn_4 for most of the rare-earth elements. Then we may assume that a valence electron concentration (VEC) is likely to dictate the stability of the RE_5X_4 and RE_4X_3 phases. If this is the case, can we stabilize the RE_4X_3 phases for tetralides through an increase in the VEC and what are the magnetic properties of such phases? As there are 17 rare-earth elements and different combinations of group 14 and 15 elements, the playing field is obviously rich. Chizhov et al. were first to test this hypothesis by exploring the $Ce_4(P_{1-x}Si_x)_{3-z}$ series through substitution on the nonmetal site.[17] Indeed, the anti-Th_3P_4 structure could be stabilized for the Ce pseudobinary through P substitution and an associated increase in the VEC. The authors estimated that an excess of 1.4−3.1 e^-/fu is required for this structure to exist.

In our study, we explored this idea further and focused on the Gd-containing phases. In this paper, we report on successful stabilization of hypothetical Gd_4Ge_3 via a VEC increase achieved through substitution of Ge with more electron-rich

Received: April 20, 2012
Published: September 14, 2012

pnictogens, P, Sb, and Bi. To emphasize stabilization of "Gd_4Ge_3", we use the $Gd_4Ge_{3-x}Pn_x$ formula instead of $Gd_4Pn_{3-x}Ge_x$, as relatively small substitution levels of $x = 0.5$ in $Gd_4Ge_{3-x}Pn_x$ yield the anti-Th_3P_4 structure. We also present magnetic properties of the newly discovered $Gd_4Ge_{3-x}Pn_x$ phases and discuss their changes with respect to the size and valence electron concentration.

EXPERIMENTAL SECTION

2.1. Synthesis and X-ray Analysis. Synthesis of the $Gd_4Ge_{3-x}P_x$ ($x = 0.5$, 1, 1.5) samples was a three-step process. First, equimolar amounts of Gd (99.99 wt %, distilled grade, Metall Rare Earth Limited, China) and Ge (99.9999 wt %, Alfa Aesar) pieces were arc melted. The binary was then ground into a powder in an Ar-filled drybox and mixed with P (99.999 wt %, Puratronic, Alfa Aesar) powder to produce a 1:1 molar ratio of the GdGe:P precursor. The resultant powder was pressed, sealed in an evacuated silica tube, and heated as described in ref 18. The product was checked by powder X-ray diffraction before combining it with elemental Gd and Ge powders to yield the desired $Gd_4Ge_{3-x}P_x$ compositions. Powders with a total mass of ~1 g were pressed and arc melted at least 3 times to achieve homogeneity. No significant losses were observed. Part of the ingot from each sample was wrapped in a separated Ta foil, sealed in an evacuated silica tube, and annealed at 1173 K for 2 weeks. Ampules were then quenched in cold water.

Samples with $Gd_4Ge_{3-x}Sb_x$ and $Gd_4Ge_{3-x}Bi_x$ ($x = 0.5-3$) compositions were prepared with a $x = 0.5$ increment by arc melting ~1 g of stoichiometric elemental Gd, Ge, and Sb (99.999 wt %, CERAC Inc.) or Bi (99.998 wt %, Alfa Aesar) pieces and then remelting them at least 3 times to ensure homogeneity. Excess of Sb or Bi (1–10 wt %, larger excess for the more Sb- and Bi-rich samples) was loaded to compensate for their losses during arc melting, which resulted in less than 3 wt % total losses for all samples. Cast samples were wrapped in individual Ta foils, sealed in silica ampules, and annealed at 1273 K for at least 1 month to improve crystallinity and homogeneity. Ampules were then quenched in cold water.

Room-temperature phase analyses of the polycrystalline samples were performed on a PANalytical X'Pert Pro diffractometer with a linear X'Celerator detector using Co Kα radiation in the 2θ range from 20° to 90°. Lattice parameters were refined using the FullProf software.[19] All samples adopt the cubic anti-Th_3P_4-type structure with space group *I*-43*d*. Gd and *Pn* atoms sit on the 16*c* (x, x, x) and 12*a* (0, 0.25, 0.375) sites, respectively. The refined powder pattern for the Gd_4Bi_3 sample is shown in the Supporting Information, Figure S1. The lattice parameter of 9.38756(2) Å and atomic coordinate $x = 0.0721(1)$ for the Gd atoms were extracted. These values agree well with literature ones.[6,20,21] Single crystals extracted from the $Gd_4Ge_{2.5}P_{0.5}$, $Gd_4Ge_{3-x}Sb_x$ ($x = 1$, 1.5, 2, 2.5, 3), and $Gd_4Ge_{3-x}Bi_x$ ($x = 0.5$, 1, 1.5, 2) samples were analyzed on a STOE IPDS II diffractometer with Mo Kα radiation.[22] No crystals suitable for X-ray analysis could be picked up from the $Gd_4Ge_{3-x}Bi_x$ samples with $x = 2.5$ and 3. Structures were solved and refined using the SHELXS and SHELXL software packages, respectively.[23] All crystals adopt the cubic anti-Th_3P_4-type structure with the *I*-43*d* space group. The Gd and Ge/*Pn* atoms occupy the 16*c* and 12*a* sites, respectively. Refinement of the Ge/*Pn* occupancies proceeded well due to the significant differences in the atomic scattering factors between Ge and P, Sb, or Bi. Crystallographic data and refinement details for $Gd_4Ge_{2.5}P_{0.5}$, $Gd_4Ge_{2.5}Bi_{0.5}$, and Gd_4Ge_2Sb single crystals are summarized in Tables 1 and 2, and those for other crystals are provided in the Supporting Information, Tables S1–S4. Further details of the crystal structure investigated are available from the Fachinformationszentrum Karlsruhe, 76344 Eggenstein-Leopoldshafen, Germany, on quoting depository number CSD-424230 for $Gd_4Ge_{2.51}P_{0.49}$, 424231 for $Gd_4Ge_{2.49}Bi_{0.51}$, 424232 for $Gd_4Ge_{1.97}Sb_{1.03}$, and 424233-39 for the ones listed in the Supporting Information.

Lattice parameters obtained from single-crystal X-ray diffraction are plotted vs the refined *Pn* amounts in Figure 1. For the $Gd_4Ge_{0.5}Bi_{2.5}$ and Gd_4Bi_3 samples, the lattice parameters derived from the powder data were plotted and the loading composition of $Gd_4Ge_{0.5}Bi_{2.5}$ was used in the graph. For the Bi series, no standard deviation in composition was included for $Gd_4Ge_{0.5}Bi_{2.5}$ because the Ge/Bi occupancy could not be reliably determined from the Rietveld refinement.

Table 1. Crystallographic Data and Refinement Results for $Gd_4Ge_{2.51(5)}P_{0.49(5)}$, $Gd_4Ge_{2.49(3)}Bi_{0.51(3)}$, and $Gd_4Ge_{1.97(4)}Sb_{1.03(4)}$ Single Crystals

	$Gd_4Ge_{2.5}P_{0.5}$	$Gd_4Ge_{2.5}Bi_{0.5}$	Gd_4Ge_2Sb
refined composition	$Gd_4Ge_{2.51(5)}P_{0.49(5)}$	$Gd_4Ge_{2.49(3)}Bi_{0.51(3)}$	$Gd_4Ge_{1.97(4)}Sb_{1.03(4)}$
space group	*I*-43*d*	*I*-43*d*	*I*-43*d*
lattice params *a*, Å	8.8348(6)	8.9799(9)	9.0111(5)
vol., Å^3	689.59(8)	724.1(1)	731.70(7)
cryst size, mm^3	0.028 × 0.047 × 0.047	0.013 × 0.054 × 0.113	0.016 × 0.045 × 0.103
2θ range for data collection, deg	11.3–58.16	11.12–58.40	11.08–58.18
index ranges	$-12 \le h \le 9$	$-12 \le h \le 12$	$-11 \le h \le 12$
	$-12 \le k \le 12$	$-10 \le k \le 12$	$-10 \le k \le 12$
	$-12 \le l \le 12$	$-12 \le l \le 11$	$-12 \le l \le 12$
reflns collected	3312	3723	3804
independent reflns	161 [R(int) = 0.0454]	169 [R(int) = 0.1559]	176 [R(int) = 0.0540]
completeness to max 2θ (%)	100.0	99.0	100.0
data/restraints/parameters	161/0/8	169/0/9	172/0/9
goodness-of-fit on F^2	1.110	1.142	1.255
final R indices [$I > 2\sigma(I)$]	R_1 = 0.0224, wR_2 = 0.0468	R_1 = 0.0281, wR_2 = 0.0458	R_1 = 0.0161, wR_2 = 0.0212
R indices (all data)	R_1 = 0.0272, wR_2 = 0.0483	R_1 = 0.0435, wR_2 = 0.0481	R_1 = 0.0221, wR_2 = 0.0218
extinction coefficient	0.0008(2)	0.00027(17)	0.00006(4)
largest diff. peak and hole (e/Å^{-3})	0.800 and −0.801	1.526 and −1.244	0.574 and −0.668

2.2. Quantitative Elemental Analysis. Elemental compositions of the $Gd_4Ge_{3-x}Sb_x$ ($x = 1-2.5$) and $Gd_4Ge_{3-x}Bi_x$ ($x = 0.5-2.5$) samples were examined through wavelength-dispersive spectroscopy (WDS) on a JEOL 8900 electron probe microanalyzer (EPMA). Due to the overlap between the Gd Lα and the Ge Lα lines, only the *Pn* (*Pn* = Sb, Bi) compositions could be accurately determined. Ge compositions were estimated assuming that Ge and *Pn* atoms fully occupied the 12*a* sites and the Gd atoms fully occupied the 16*c* site. To verify the validity of the EPMA results, additional elemental analysis on the $Gd_4Ge_{3-x}Sb_x$ ($x = 1-2.5$) series was performed using a Resonetics M-50-Lr 193 nm Excimer laser ablation system coupled to an Agilent 7700x quadrupole ICP-MS with a 32 μm spot size. Pure Gd_5Ge_4 and Gd_4Sb_3 binaries were used as internal standards. Results are listed in Table 3.

2.3. Band Structure Calculations. Tight-binding, linear-muffin-tin-orbital (TB-LMTO) electronic structure calculations were performed with the Stuttgart program[24] for the Gd_4Sb_3, Gd_4Bi_3, hypothetical "Gd_4Ge_3", and Gd_5Ge_4 binary phases using the atomic sphere approximation (ASA).[25] As mentioned, the former three binaries adopt the cubic anti-Th_3P_4-type structure. The atomic coordinates for Gd range from $x = 0.0660$ to 0.0721, and the Ge/Sb/Bi atoms are fixed on the 12*a* (0, 0.25, 0.375) site. Lattice parameters and atomic coordinates for the Gd_4Sb_3 and Gd_4Bi_3 structures were extracted from single-crystal and powder X-ray refinements, respectively. For "Gd_4Ge_3", the lattice parameter a = 8.89 Å was extrapolated from the single-crystal X-ray data of $Gd_4Ge_{3-x}Pn_x$ (*Pn* = P, Sb, Bi) (Figure 1). The atomic coordinates for Gd (0.0660, 0.0660, 0.0660), were estimated based on the single crystal refinement data of $Gd_4Ge_{3-x}Pn_x$ (*Pn* = P, Bi; $x = 0.5$). For orthorhombic Gd_5Ge_4 (*Pnma*), lattice parameters and atomic coordinates were taken from Yao et al.[26] Local density approximation

dx.doi.org/10.1021/ic300817j | Inorg. Chem. 2012, 51, 10169–10175

Table 2. Atomic and Isotropic Temperature Parameters (U, Å^2) for $Gd_4Ge_{2.51(5)}P_{0.49(5)}$, $Gd_4Ge_{2.49(3)}Bi_{0.51(3)}$, and $Gd_4Ge_{1.97(4)}Sb_{1.03(4)}$ Single Crystals

atom	site	occupancy	x/a	y/b	z/c	U
$Gd_4Ge_{2.51(5)}P_{0.49(5)}$						
Gd	16*c*	1	0.0660(1)	0.0660(1)	0.0660(1)	0.012(1)
Ge/P	12*a*	0.84(2)/0.16 (2)	0	1/4	3/8	0.012(1)
$Gd_4Ge_{2.49(3)}Bi_{0.51(3)}$						
Gd	16*c*	1	0.0667(1)	0.0667(1)	0.0667(1)	0.020(1)
Ge/Bi	12*a*	0.831/0.169(9)	0	1/4	3/8	0.016(1)
$Gd_4Ge_{1.97(4)}Sb_{1.03(4)}$						
Gd	16*c*	1	0.0680(1)	0.0680(1)	0.0680(1)	0.015(1)
Ge/Sb	12*a*	0.66/0.34(1)	0	1/4	3/8	0.010(1)

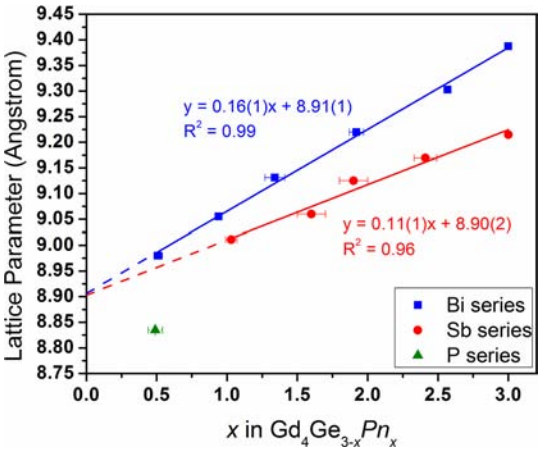

Figure 1. Lattice parameters vs *Pn* amount in $Gd_4Ge_{3-x}Pn_x$ (*Pn* = P, Sb, Bi; x = 0.5−3). Symbols with the error bars represent compositions obtained from single-crystal refinements. For x = 0.5 and 1 in the Bi series, error bars are too small to be observed.

(LDA)[27] was used to treat exchange and correlation interactions. Space-filling empty spheres were introduced into the Wigner−Seitz (WS) cell to achieve convergence during the calculation. Radii for the WS cell were generated automatically, and the radii used for $Gd_4(Ge/Sb/Bi)_3$ were Gd = 3.35−3.42 Å, Ge = 2.94 Å, Sb = 3.21 Å, and Bi = 3.30 Å. The basis set included 6s and 5d orbitals for Gd and *n*s and *n*p orbitals for Ge/Sb/Bi (n = 4, 5, and 6). Two empty spheres (E) with WS radii of 1.43−2.11 Å were included in each binary for calculation. Orbitals were treated using the Löwdin downfolding technique.[24,25] The first Brillouin zone for the reciprocal space integration included 512 irreducible k points. The Gd 4f orbitals were treated as core ones that do not participate in bonding. Orbital interactions were analyzed via partial density of states (PDOS) and crystal orbital Hamilton population (COHP) calculations using the tetrahedron method.[28] For the COHP calculations, the maximum distance considered between two Gd atoms was 4.21 Å.

2.3. Magnetic Measurements. Magnetic measurements were performed for polycrystalline $Gd_4Ge_{3-x}Pn_x$ samples (*Pn* = P, x = 0.5; *Pn* = Sb, x = 1, 1.5, 2, 2.5, 3; *Pn* = Bi, x = 0.5, 1, 1.5, 2, 2.5, 3) with a 100 Oe external field in a field-cooled (FC) mode from 5 to 400 K with 2−5 K increments on a Quantum Design Superconducting Quantum Interference Device (SQUID) instrument. Magnetization (M) vs temperature (T) data are shown in Figure 2.

RESULTS AND DISCUSSION

3.1. Composition and Stability of $Gd_4Ge_{3-x}Pn_x$. From powder X-ray analysis, the prereacted GdGe:P precursor was confirmed to contain the GdP binary and elemental Ge. Formation of the stable GdP binary prior to arc melting the $Gd_4Ge_{3-x}P_x$ (x = 0.5−1.5) samples is essential for minimizing P losses and allowing formation of desired phases. The cubic anti-Th_3P_4 phase was present in all cast samples, but its amount decreased for larger P amounts and after annealing (Supporting Information Table S5). Interestingly, annealing the x = 0.5 sample at 900 °C increased the amount of $Gd_4Ge_{3-x}P_x$ phase and led to decomposition of Gd_5Ge_4 found in the cast sample. However, this had a minimal effect on the presence of the Gd_5Ge_3 impurity. This observation suggests that P stabilizes the "Gd_4Ge_3" and not Gd_5Ge_4 phase. The P amount does not appear to extend beyond x = 0.49(5) (based on single-crystal results) since annealing of the x = 1 and 1.5 samples either reduced the amount of the desired phase or eliminated it completely. One may question whether P is really present in the $Gd_4Ge_{3-x}P_x$ phase. First, the pure Gd_4Ge_3 phase does not exist. Second, the lattice parameter (8.8348(6) Å) of $Gd_4Ge_{2.51}P_{0.49}$ is smaller than those extrapolated from the $Gd_4Ge_{3-x}Sb_x$ and $Gd_4Ge_{3-x}Bi_x$ series for the hypothetical Gd_4Ge_3 binary (8.90(2) and 8.91(1) Å, Figure 1). Therefore, $Gd_4Ge_{2.51}P_{0.49}$ exists and is stabilized through P substitution.

As for the $Gd_4Ge_{3-x}Sb_x$ (x = 0.5−3) series, the anti-Th_3P_4 structure was observed in the cast and annealed samples with $1 \leq x \leq 3$. On the basis of the refinement results, the x = 0.5 sample contained exclusively Gd_5Ge_3 and Gd_5Ge_4 phases and further annealing promoted formation of GdGe and Sb impurities. In the $Gd_4Ge_{3-x}Bi_x$ (x = 0.5−3) series, the anti-Th_3P_4 structure was observed in all cast and annealed samples.

Table 3. Compositions Based on the EPMA, LA-ICP-MS, and the X-ray Single-Crystal Analyses[a]

	Pn = Sb			*Pn* = Bi	
loading	EPMA	LA-ICP-MS	X-ray	EPMA	X-ray
$Gd_4Ge_{2.5}Pn_{0.5}$	N/A	N/A	N/A	$Gd_4Ge_{2.46(8)}Bi_{0.54(8)}$	$Gd_4Ge_{2.49(3)}Bi_{0.51(3)}$
Gd_4Ge_2Pn	$Gd_4Ge_{1.9(1)}Sb_{1.1(1)}$	$Gd_{4.0(2)}Ge_{2.04(5)}Sb_{1.00(2)}$	$Gd_4Ge_{1.97(4)}Sb_{1.03(4)}$	$Gd_4Ge_{1.95(2)}Bi_{1.05(2)}$	$Gd_4Ge_{2.07(2)}Bi_{0.93(2)}$
$Gd_4Ge_{1.5}Pn_{1.5}$	$Gd_4Ge_{1.6(2)}Sb_{1.4(2)}$	$Gd_{4.0(2)}Ge_{1.49(3)}Sb_{1.47(3)}$	$Gd_4Ge_{1.4(1)}Sb_{1.6(1)}$	$Gd_4Ge_{1.48(4)}Bi_{1.52(4)}$	$Gd_4Ge_{1.66(7)}Bi_{1.34(7)}$
Gd_4GePn_2	$Gd_4Ge_{0.93(6)}Sb_{2.07(6)}$	$Gd_{4.0(2)}Ge_{1.01(2)}Sb_{2.02(4)}$	$Gd_4Ge_{1.1(1)}Sb_{1.9(1)}$	$Gd_4Ge_{1.1(1)}Bi_{1.9(1)}$	$Gd_4Ge_{1.08(5)}Bi_{1.92(5)}$
$Gd_4Ge_{0.5}Pn_{2.5}$	$Gd_4Ge_{0.59(4)}Sb_{2.41(4)}$	$Gd_{4.0(2)}Ge_{0.48(1)}Sb_{2.58(5)}$	$Gd_4Ge_{0.59(8)}Sb_{2.41(8)}$	$Gd_4Ge_{0.88(4)}Bi_{2.12(4)}$	N/A

[a]For EPMA results, Ge compositions are estimated using the *Pn* concentrations.

dx.doi.org/10.1021/ic300817j | Inorg. Chem. 2012, 51, 10169−10175

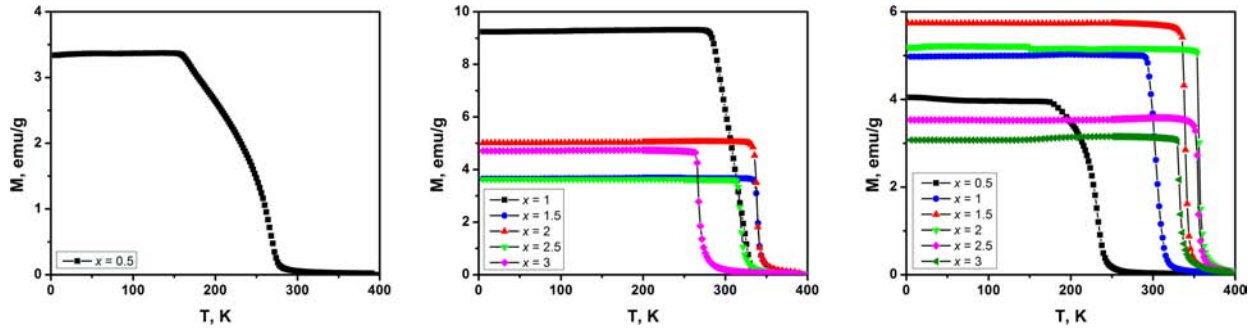

Figure 2. Magnetization vs temperature plots for $Gd_4Ge_{2.5}P_{0.5}$ (left), $Gd_4Ge_{3-x}Sb_x$ (x = 1−3) (center), and $Gd_4Ge_{3-x}Bi_x$ (x = 0.5−3) (right).

On the basis of single-crystal refinements and powder analysis, the homogeneity regions for $Gd_4Ge_{3-x}Sb_x$ extend from x = 1.03(4) to 3 and for $Gd_4Ge_{3-x}Bi_x$ from x = 0.51(3) to 3. Using the lattice parameters for $Gd_4Ge_{3-x}Sb_x$ and $Gd_4Ge_{3-x}Bi_x$, one can extrapolate the lattice parameters for hypothetical Gd_4Ge_3, which are 8.90(2) and 8.91(1) Å, respectively. It is worth mentioning that a small substitution level of Bi (x = 0.51(3)), similar to P substitution, is sufficient to stabilize the anti-Th_3P_4 structure. Formation of the Sb- and Bi-rich $Gd_4Ge_{3-x}Pn_x$ phases is not surprising, as the Gd_4Sb_3 and Gd_4Bi_3 binaries are stable, so these mixed phases can be seen as Ge-substituted binaries. However, for small Sb and Bi amounts such as $0.5 \leq x \leq 1$ the composition resemblance to Gd_4Sb_3 and Gd_4Bi_3 is lost. In fact, the Ge-rich $Gd_4Ge_{3-x}Sb_x$ and $Gd_4Ge_{3-x}Bi_x$ should be better treated as derivatives of hypothetical Gd_4Ge_3. This argument applies even better to $Gd_4Ge_{2.51}P_{0.49}$, as Gd_4P_3 and P-rich $Gd_4Ge_{3-x}P_x$ phases do not exist, and thus, any P present can be seen as substitution for Ge in "Gd_4Ge_3".

One issue that we have to address is possible deficiencies on the 12*a* site in $Gd_4Ge_{3-x}Pn_x$. Studies on $Ce_4(P_{1-x}Si_x)_{3-z}$ indicated that the 12*a* site may be deficient up to z = 0.34(3), but no correlation with either the P or the Si amount could be established.[17] In our case, only the Sb/Bi concentration could be reliably established from EPMA analysis, so the Ge amount was calculated assuming a full occupancy of the 12*a* site (Table 3). While the EPMA compositions can be used only as a guide, they suggest that the Sb/Bi amounts are within three standard deviations from the loading ones except for the $Gd_4Ge_{0.5}Bi_{2.5}$ sample. Additional LA-ICP-MS analysis conducted on the $Gd_4Ge_{3-x}Sb_x$ series confirmed that there are no deficiencies present in this system. These EPMA and LA-ICP-MS results are supported by the X-ray single-crystal ones, which also yielded compositions close to the loading ones (Table 3) and did not indicate deficiencies on the 12*a* site. On the basis of the above analyses, we suggest that the 12*a* site is fully populated and if the deficiencies are present they are likely to be small.

The anti-Th_3P_4 crystal structure consists of two distinct atomic positions. The Gd atom sits in a distorted octahedral environment surrounded by six Ge/*Pn* atoms, and each *p* element is surrounded by eight Gd neighbors. The atomic distances between the Gd and the corresponding *Pn* (*Pn* = Sb, Bi, Ge) element are listed in Table 4. Since no experimental data is available for "Gd_4Ge_3", no standard deviations are given for the calculated distances. As there are no short Ge/*Pn*−Ge/*Pn* bonds in the structure, we can treat the Ge/*Pn* atoms as anions that draw electrons from the Gd atoms. Following the Zintl−Klemm formalism for valence compounds,[29−31] we can write an electronic formula for $Gd_4Ge_{3-x}Pn_x$ as

Table 4. Experimental Distances for Gd_4Sb_3 and Gd_4Bi_3 and Calculated Ones for Gd_4Ge_3

			distances		
atom 1	atom 2	C.N.	Sb	Bi	Ge
Gd	*Pn*	3×	3.0807(4)	3.1381(9)	2.9174
	Pn	3×	3.3042(4)	3.3664(9)	3.2505
	Gd	3×	3.5374(6)	3.6040(3)	3.4756
	Gd	2×	3.9902(5)	4.065(1)	3.8495
	Gd	6×	4.4109(6)	4.493(1)	4.1920
Pn	Gd	4×	3.0807(4)	3.1381(9)	2.9174
	Gd	4×	3.3042(4)	3.3664(9)	3.2505
	Pn	8×	4.3099(2)	4.3906(1)	4.1579

$(Gd^{3+})_4(Ge^{4-})_{3-x}(Pn^{3-})_x(xe^-)$. Thus, introduction of *Pn* provides an excess of electrons and appears to stabilize the structure, considering that "Gd_4Ge_3" does not exist. On the other hand, the atomic size is unlikely to be a factor, as the same structure is observed for $Gd_4Ge_{2.5}P_{0.5}$ and $Gd_4Ge_{2.5}Bi_{0.5}$, while the atomic sizes of P (r_{cov} = 1.10 Å) and Bi (r_{cov} = 1.53 Å) differ significantly from each other and from that of Ge (r_{cov} = 1.22 Å).[32] The importance of extra electrons for the stability of the anti-Th_3P_4 structure is also supported by the anion deficiency in $La_4Ge_{2.67}$[33] and existence of $Ce_4(P_{1-x}Si_x)_{3-z}$.[17]

3.2. Electronic Structure. Using the Zintl−Klemm formalism, we can predict that the hypothetical Gd_4Ge_3 phase should be charge balanced, $(Gd^{3+})_4(Ge^{4-})_3$, and that the valence band, consisting of the Ge states, should be occupied, while the conduction band, made up of the Gd states, should be empty. The Fermi level should reside in a gap (or pseudogap) between the bands. This simple reasoning is supported by the TB-LMTO-ASA calculations. The density of states (DOS) and crystal orbital Hamilton population (COHP) for hypothetical Gd_4Ge_3 are presented in Figure 3, center. Indeed, the conduction band is dominated by Ge states while the valence bands are by Gd states, and the two are separated by a pseudogap, which corresponds to 24 e^-/fu or the Gd_4Ge_3 composition. However, some additional features became also apparent. First, the valence band has a substantial contribution from the Gd states, indicative of the significant hybridization between the Gd and the Ge orbitals. Second, there are strong bonding Gd−Gd and Gd−Ge interactions in the conduction band (Ge−Ge interactions are negligible as d_{Ge-Ge} > 4 Å). These observations suggest that the ionic picture employed for the electron count is too simplistic and that Gd−Gd interactions cannot be ignored. The fact that the interactions above the Fermi level are strongly bonding explains why *Pn* substitution is possible for hypothetical Gd_4Ge_3 and why electron-rich Gd_4Sb_3 and Gd_4Bi_3 are stable. The electronic

dx.doi.org/10.1021/ic300817j | Inorg. Chem. 2012, 51, 10169−10175

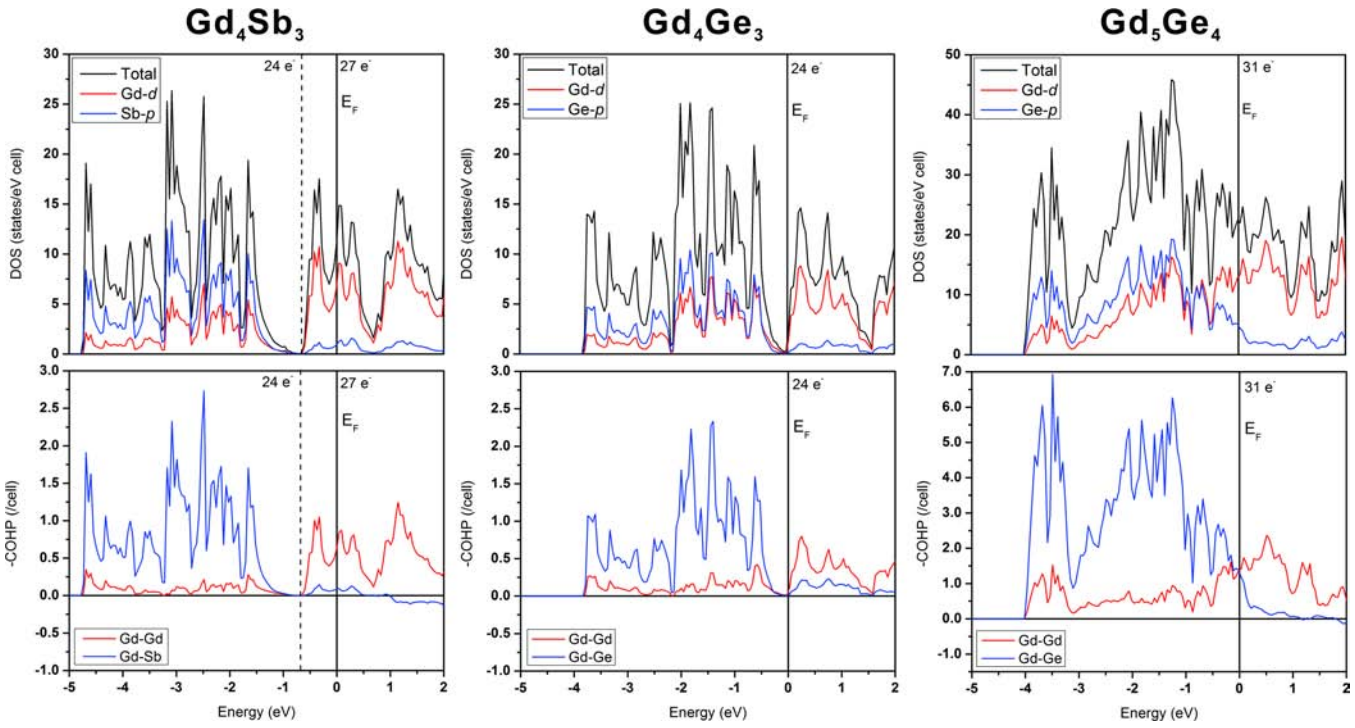

Figure 3. Density of states (DOS) and crystal orbital Hamilton population (COHP) for Gd_4Sb_3 (left), Gd_4Ge_3 (center), and Gd_5Ge_4 (right).

structures of Gd_4Sb_3 and Gd_4Bi_3 are quite similar, and only that of Gd_4Sb_3 is given in Figure 3, left. (For Gd_4Bi_3, please refer to Figure S2. Supporting Information.) There is a strong resemblance between the electronic structures of Gd_4Sb_3 and "Gd_4Ge_3", but due to the higher electron count the Fermi level for Gd_4Sb_3 resides up in the conduction band.

Finally, we want to address potential reasons of why "Gd_4Ge_3" does not exist but the compositionally close Gd_5Ge_4 phase does. We will limit our analysis to the bonding in the two phases. The electronic structure of Gd_5Ge_4 is shown in Figure 3, right. When compared to "Gd_4Ge_3", Gd_5Ge_4 displays stronger bonding Gd−Gd and Gd−Ge interactions around the Fermi level. While such interactions are also bonding in the vicinity of the Fermi level for "Gd_4Ge_3", they have no contribution at the Fermi level itself due to the presence of a pseudogap. Therefore, we may speculate that optimization of the Gd−Gd and Gd−Ge interactions is likely a key factor dictating the stability of Gd_5Ge_4. We may also argue that a VEC increase above $31e^-$/fu is not favorable for Gd_5Ge_4, as there are interslab Ge−Ge (Ge_2) dimers in this phase and interactions within them are antibonding around the Fermi level.[11] Likely, destabilization of these dimers is the reason why Gd_5Sb_4 and Gd_5Bi_4 with $35e^-$/fu do not exist.

3.3. Magnetic Properties of $Gd_4Ge_{3-x}Pn_x$.

All $Gd_4Ge_{3-x}Pn_x$ (*Pn* = P, Sb, Bi) samples are ferromagnetic with transitions temperatures (T_C) ranging from 234 to 356 K (Table 5). The effective magnetic moments (μ_B) and Weiss temperatures could not be calculated because of the small number of data points in the paramagnetic regimes. The antiferromagnetic impurities, Gd_5Ge_3 (T_N = 76 K)[34] and GdP (T_N = 16 K),[35] were not observed on the magnetization curve of $Gd_4Ge_{2.5}P_{0.5}$, which is due to their low magnetic contributions to the total magnetization. For the samples with x = 0.5, the presence of a heavier element resulted in a lower ordering temperature: T_C dropped from 270 K for $Gd_4Ge_{2.5}P_{0.5}$ to 234 K for $Gd_4Ge_{2.5}Bi_{0.5}$. This corresponds well

Table 5. Curie Temperatures (T_C, K) of $Gd_4Ge_{3-x}Pn_x$ (*Pn* = P, Sb, Bi; x = 0.5−3)

x	$Gd_4Ge_{3-x}P_x$	$Gd_4Ge_{3-x}Sb_x$	$Gd_4Ge_{3-x}Bi_x$
0.5	270	N/A	234
1	N/A	316	302
1.5	N/A	340	340
2	N/A	340	356
2.5	N/A	320	356
3	N/A	268	334

with the results obtained by Hulliger et al. for the La series, in which the T_C values decrease as bigger anions are introduced: T_C (La_4As_3) > T_C (La_4Sb_3) > T_C (La_4Bi_3).[36] However, these results contradict the ones for the $Gd_4Sb_{3-x}Bi_x$ series, where the T_C values increase upon Bi substitution.[6] Currently, we do not understand this trend for the $Gd_4Ge_{2.5}P_{0.5}$ and $Gd_4Ge_{2.5}Bi_{0.5}$ samples.

Curie temperature as a function of the *Pn* concentration for the $Gd_4Ge_{3-x}Sb_x$ and $Gd_4Ge_{3-x}Bi_x$ series is plotted in Figure 4. The T_C values display an interesting parabolic behavior which to our knowledge was not observed for the RE_4Pn_3 phases before. According to Ruderman−Kittel−Kasuya−Yosida (*RKKY*) theory,[37−39] such peculiar tendency may result from changes in the valence electron concentration and variations in the Gd−Gd distances, both of which are controlled by substitution levels of the *p* element. Most likely, a rise in the T_C values for small x values can be attributed to an increase in the number of conduction electrons (higher density of states) as the Fermi level moves from the pseudogap in "Gd_4Ge_3" into the conduction band in $Gd_4Ge_{3-x}Pn_x$ (see band structure of Gd_4Sb_3 in Figure 3). Also, the atomic sizes may play a role in this concentration region, as an increase in the T_C values for $Gd_4Ge_{3-x}Bi_x$ is steeper than that for $Gd_4Ge_{3-x}Sb_x$. As x increases further, the Fermi level reaches the maximum in the DOS for both series (at ca. −0.33 and −0.29 eV for Gd_4Sb_3 and

dx.doi.org/10.1021/ic300817j | Inorg. Chem. 2012, 51, 10169−10175

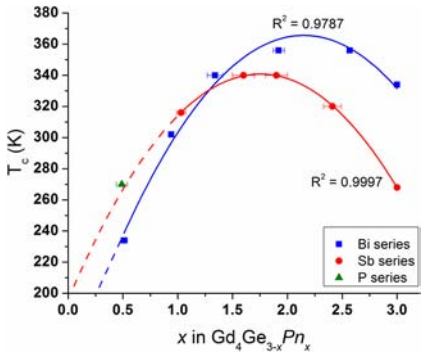

Figure 4. Curie temperatures (T_C) as a function of the *Pn* amount for $Gd_4Ge_{3-x}Pn_x$ (*Pn*: P, Sb, Bi; x = 0–3). Symbols with the error bars represent compositions obtained from single-crystal refinements. For x = 0.5 and 1 in the Bi series, error bars are too small to be observed.

Gd_4Bi_3), which corresponds to ca. 25.5 e^-/fu or the $Gd_4Ge_{1.5}Pn_{1.5}$ composition (*Pn* = Sb, Bi). This agrees reasonably well with the high T_C values observed for $Gd_4Ge_{1.5}Sb_{1.5}$ and Gd_4GeSb_2. However, the maximum Curie temperatures for the Bi series is shifted to higher x = 2 and 2.5, which may be due to the inadequacy of the rigid band model used for these arguments or due to the fact that experimental and calculated DOSs are somewhat different. As x increases further, the DOS diminishes, and this explains lower T_C values for the Sb- and Bi-rich phases. Again, the size of the *p* element appears to be important as the $Gd_4Ge_{3-x}Bi_x$ series has a smaller decline in the T_C values.

CONCLUSIONS

While the "Gd_4Ge_3" binary does not exist, it can be easily stabilized by an increase in the valence electron count (VEC) achieved through substitution of more electron-rich P, Sb, or Bi for Ge. Even a relatively small increase of 0.5 e^- in the VEC is sufficient to stabilize the $Gd_4Ge_{2.5}P_{0.5}$ and $Gd_4Ge_{2.5}Bi_{0.5}$ pseudobinary phases with the anti-Th_3P_4 structure. Larger substitution levels up to the end members are possible for the $Gd_4Ge_{3-x}Sb_x$ and $Gd_4Sb_{3-x}Bi_x$ series. Electronic structure analysis reveals that extra electrons in excess of 24 e^-/fu, corresponding to the charge-balanced $(Gd^{3+})_4(Ge^{4-})_3$ formula, populate the bonding Gd–Gd and Gd–Ge interactions and thus stabilize the anti-Th_3P_4 structure. A likely reason for the nonexistence of pure "Gd_4Ge_3" is the presence of the compositionally close Gd_5Ge_4 phase with strong Gd–Gd and Gd–Ge interactions around the Fermi level.

All $Gd_4Ge_{3-x}Pn_x$ (*Pn* = P, Sb, Bi; x = 0.5–3) phases order ferromagnetically with relatively high Curie temperatures (T_C = 234–356 K). A parabolic behavior in the T_C values for the $Gd_4Ge_{3-x}Sb_x$ and $Gd_4Sb_{3-x}Bi_x$ series is mostly due to changes in the numbers of conduction electrons, associated with Ge/Sb(Bi) substitution.

ASSOCIATED CONTENT

Supporting Information

This material is available free of charge via the Internet at http://pubs.acs.org.

AUTHOR INFORMATION

Corresponding Author

*E-mail: mozhar@mcmaster.ca.

Notes

The authors declare no competing financial interest.

REFERENCES

(1) Misra, S.; Miller, G. J. *J. Am. Chem. Soc.* **2008**, *130*, 13900–13911.
(2) Morellon, L.; Magen, C.; Algarabel, P. A.; Ibarra, M. R.; Ritter, C. *Appl. Phys. Lett.* **2001**, *79*, 1318–1320.
(3) Ritter, C.; Morellon, L.; Algarabel, P. A.; Magen, C.; Ibarra, M. R. *Phys. Rev. B* **2002**, *65*, 094405/094401–094405/094410.
(4) Wu, L. M.; Kim, S. H.; Seo, D. K. *J. Am. Chem. Soc.* **2005**, *127*, 15682–15683.
(5) Tobash, P. H.; Bobev, S. *J. Am. Chem. Soc.* **2006**, *128*, 3532–3533.
(6) Niu, X. J.; Gschneidner, K. A., Jr.; Pecharsky, A. O.; Pecharsky, V. K. *J. Magn. Magn. Mater.* **2001**, *234*, 193–206.
(7) Pecharsky, V. K.; Gschneidner, K. A., Jr. *Phys. Rev. Lett.* **1997**, *78*, 4494–4497.
(8) Levin, E. M.; Gschneidner, K. A., Jr.; Pecharsky, V. K. *J. Magn. Magn. Mater.* **2001**, *231*, 135–145.
(9) Pecharsky, V. K.; Gschneidner, K. A., Jr. *Adv. Mater.* **2001**, *13*, 683–686.
(10) Pecharsky, V. K.; Holm, A. P.; Gschneidner, K. A., Jr.; Rink, R. *Phys. Rev. Lett.* **2003**, *91*, 197204.
(11) Mozharivskyj, Y.; Choe, W.; Pecharsky, A. O.; Miller, G. J. *J. Am. Chem. Soc.* **2003**, *125*, 15183–15190.
(12) Svitlyk, V.; Cheung, Y. Y. J.; Mozharivskyj, Y. *J. Magn. Magn. Mater.* **2010**, *322*, 2558–2566.
(13) Svitlyk, V.; Miller, G. J.; Mozharivskyj, Y. *J. Am. Chem. Soc.* **2009**, *131*, 2367–2374.
(14) Svitlyk, V.; Campbell, B. J.; Mozharivskyj, Y. *Inorg. Chem.* **2009**, *48*, 10364–10370.
(15) Misra, S.; Mozharivskyj, Y.; Tsokol, A. O.; Schlagel, D. L.; Lograsso, T. A.; Miller, G. J. *J. Solid State Chem.* **2009**, *182*, 3031–3040.
(16) In *Pearson's Handbook of Crystallographic Data for Intermetallic Phases*; Villars, P., Calvert, L. D., Eds.; ASM International: Materials Park, OH, 1991.
(17) Chizhov, P. S.; Khasanova, N. R.; Baitinger, M.; Schnelle, W.; Prots, Y.; Burkhardt, U.; Antipov, E. V.; Grin, Y. *Inorg. Chem.* **2006**, *45*, 7210–7216.
(18) Svitlyk, V.; Mozharivskyj, Y. *Solid State Sci.* **2009**, *11*, 1941–1944.
(19) Rodriguez-Carvajal, J. *IUCR Newslett.* **2001**, *26*, 12–19.
(20) Gambino, R. J. *J. Less-Common Met.* **1967**, *12*, 344–352.
(21) Yoshihara, K.; Taylor, J. B.; Calvert, L. D.; Despault, J. G. *J. Less-Common Met.* **1975**, *41*, 329–337.
(22) *STOE*, 2.05 ed.; STOE & Cie GmbH: Darmstadt, Germany, 2004.
(23) Sheldrick, G. M. *SHEXL97 and SHELXS97*; University of Göttigen: Göttigen, Germany, 1997.
(24) Jepsen, O.; Burkhardt, A.; Andersen, O. K. *The TB-LMTO-ASA Program*, 4.7 ed.; Max-Planck-Institut fr Festkreperforschung: Stuttart, Germany, 1999.
(25) Lambrecht, W. R. L.; Andersen, O. K. *Phys. Rev. B* **1986**, *34*, 2439.
(26) Yao, J.; Wang, P.; Mozharivskyj, Y. *Chem. Mater.* **2012**, *24* (3), 552–556.
(27) Andersen, O. K.; Jepsen, O. *Phys. Rev. Lett.* **1984**, *53*, 2571.
(28) Blöchl, P. E.; Jepsen, O.; Andersen, O. K. *Phys. Rev. B* **1994**, *49*, 16223.
(29) Zintl, E. *Angew. Chem.* **1939**, *52*, 1.
(30) Schäfer, H.; Eisenmann, B.; Muller, W. *Angew. Chem., Int.Ed.* **1973**, *12*, 694.
(31) *Chemistry, Structure and Bonding of Zintl Phases and Ions*; Kauzlarich, S. M., Ed.; VCH Publishers: New York, 1996.
(32) Pauling, L. C. *The Nature of the Chemical Bond and the Structure of Molecules and Crystals: An Introduction to Modern Structural Chemistry*, 3rd ed.; Cornell University Press: Ithaca, NY, 1960.

(33) Lynchak, K. A.; Kuz'ma, Yu. B.; Koslapova, T. Ya. *Poroshk. Mer. (Kiev)* **1968**, *12* (72), 42−44.
(34) Tsutaoka, T.; Nishiume, Y.; Tokunaga, T. *J. Magn. Magn. Mater.* **2004**, *272*−*276*, e421−e422.
(35) Treece, R.; Conklin, J.; Kaner, R. B. *Inorg. Chem.* **1994**, *33*, 5701−5707.
(36) Hulliger, F.; Ott, H. R. *J. Less-Common Met.* **1977**, *55*, 103−113.
(37) Kasuya, T. *Prog. Theor. Phys.* **1956**, *16*, 45.
(38) Ruderman, M. A.; Kittel, C. *Phys. Rev.* **1954**, *96*, 99−102.
(39) Yosida, K. *Phys. Rev.* **1957**, *106*, 893−898.